Structural basis of a potent human monoclonal antibody against Zika virus targeting a quaternary epitope

Feng Long[a], Michael Doyle[b], Estefania Fernandez[c,d], Andrew S. Miller[a], Thomas Klose[a], Madhumati Sevvana[a], Aubrey Bryan[e], Edgar Davidson[e], Benjamin J. Doranz[e], Richard J. Kuhn[a,f], Michael S. Diamond[c,d,g], James E. Crowe Jr.[b,h,i], and Michael G. Rossmann[a,1]

[a]Department of Biological Sciences, Purdue University, West Lafayette, IN 47907; [b]Department of Pathology, Microbiology and Immunology, Vanderbilt University, Nashville, TN 37232; [c]Department of Medicine, Washington University School of Medicine, St. Louis, MO 63110; [d]Department of Pathology & Immunology, Washington University School of Medicine, St. Louis, MO 63110; [e]Integral Molecular Inc., Philadelphia, PA 19104; [f]Purdue Institute for Inflammation, Immunology and Infectious Disease, Purdue University, West Lafayette, IN 47907; [g]Department of Molecular Microbiology, Washington University School of Medicine, St. Louis, MO 63110; [h]Department of Pediatrics, Vanderbilt University Medical Center, Nashville, TN 37232; and [i]The Vanderbilt Vaccine Center, Vanderbilt University Medical Center, Nashville, TN 37232

Edited by Wah Chiu, Stanford University, Stanford, CA, and approved December 11, 2018 (received for review September 7, 2018)

Zika virus (ZIKV) is a major human pathogen and member of the *Flavivirus* genus in the Flaviviridae family. In contrast to most other insect-transmitted flaviviruses, ZIKV also can be transmitted sexually and from mother to fetus in humans. During recent outbreaks, ZIKV infections have been linked to microcephaly, congenital disease, and Guillain-Barré syndrome. Neutralizing antibodies have potential as therapeutic agents. We report here a 4-Å-resolution cryo-electron microscopy structure of the ZIKV virion in complex with Fab fragments of the potently neutralizing human monoclonal antibody ZIKV-195. The footprint of the ZIKV-195 Fab fragment expands across two adjacent envelope (E) protein protomers. ZIKV neutralization by this antibody is presumably accomplished by cross-linking the E proteins, which likely prevents formation of E protein trimers required for fusion of the viral and cellular membranes. A single dose of ZIKV-195 administered 5 days after virus inoculation showed marked protection against lethality in a stringent mouse model of infection.

Zika virus | monoclonal antibody | membrane-fusion inhibition | neutralization mechanism | cryo-EM structure

Zika virus (ZIKV) belongs to the *Flavivirus* genus of the Flaviviridae family. Several other major human pathogens are flaviviruses including dengue (DENV), West Nile (WNV), yellow fever (YFV), Japanese encephalitis (JEV), and tick-borne encephalitis (TBEV) viruses (1). Although *Aedes* mosquitos are the primary vectors for ZIKV transmission to humans, ZIKV also can be acquired through sexual contact and blood transfusion and from pregnant mother to fetus (2). Over the past 3 y, local transmission has been confirmed in 68 countries and territories with an estimation of 3–4 million cases of ZIKV infection (3, 4). Although ZIKV infection of humans principally causes mild febrile symptoms, the recent epidemic was linked to severe neurological diseases, including congenital microcephaly and Guillain-Barré syndrome in adults (5, 6). There is no licensed vaccine or treatment currently available for ZIKV infections.

Mature ZIKV virions have similar structural features to other flaviviruses (7–11). The ZIKV particle contains an ∼11-kilobase, single-stranded, positive-sense genomic RNA enclosed by a capsid core, a membrane, and an icosahedral glycoprotein shell. The mature ZIKV virion has a diameter of ∼500 Å and consists of 180 copies each of envelope (E) and membrane (M) proteins, with each icosahedral asymmetric unit containing three E–M protein heterodimers. On the surface of a smooth mature virion, there are 30 herringbone-like rafts, with each raft formed by six E–M protein heterodimers lying antiparallel to each other (Fig. 1*A*). In comparison with DENV serotype 2 (12, 13), the mature ZIKV structure is more thermally stable (9).

The ectodomain of the E protein is divided into three domains, designated DI, DII, and DIII (Fig. 1*B*), which are responsible for cell attachment, membrane fusion, and antigenicity (14). The E proteins undergo multiple major conformational and organizational changes during entry, assembly, and maturation of the virus (15–18). Flaviviruses enter host cells through endocytosis following receptor-mediated cell attachment. In the acidic environment of endosomes, transition of the dimerized E proteins into trimers initiates viral–host membrane fusion. After the viral genomic RNA is released into the cytosol of host cells, viral proteins are synthesized. The precursor M (prM) and E proteins assemble as immature viruses in the endoplasmic reticulum by forming 60 trimeric spikes of prM–E protein heterodimers on the viral surface (19). Maturation of viruses begins in the trans-Golgi network and involves the furin cleavage of the prM protein into the pr peptide and M protein, followed by the rearrangement of the E and prM proteins into 90 dimers to form a herringbone pattern. After secretion of prematured viruses, the

Significance

Zika virus (ZIKV) has reemerged recently to cause serious human disease. However, there is no licensed vaccine or treatment currently available for ZIKV infections. Potently neutralizing antibodies are of interest due to their prophylactic and therapeutic potential. Here, we show that ZIKV-195, a potently neutralizing human monoclonal antibody, has postexposure therapeutic activity against ZIKV infection in a mouse model. We further describe the near-atomic resolution structure of the ZIKV virion in complex with ZIKV-195 Fab fragments and suggest a neutralization mechanism.

Author contributions: F.L., B.J.D., R.J.K., M.S.D., J.E.C., and M.G.R. designed research; F.L., M.D., E.F., A.S.M., A.B., and E.D. performed research; F.L., M.D., E.F., T.K., M.S., E.D., B.J.D., R.J.K., M.S.D., J.E.C., and M.G.R. analyzed data; and F.L., E.D., B.J.D., R.J.K., M.S.D., J.E.C., and M.G.R. wrote the paper.

Conflict of interest statement: J.E.C. has served as a consultant for Takeda Vaccines, Sanofi Pasteur, Pfizer, and Novavax; is on the Scientific Advisory Boards of CompuVax, GigaGen, and Meissa Vaccines; and is Founder of IDBiologics, Inc. Vanderbilt University has a patent application pending that pertains in part to the ZIKV-195 antibody. M.S.D. is a consultant for Inbios and is on the Scientific Advisory Board of Moderna. A.B., E.D., and B.J.D. are employees of Integral Molecular. B.J.D. is a shareholder of Integral Molecular.

This article is a PNAS Direct Submission.

Data deposition: The cryo-EM map and coordinates of ZIKV in complex of Fab ZIKV-195 have been deposited in the Electron Microscopy Data Bank (accession no. EMD-9131) and the Protein Data Bank (accession no. 6MID).

[1]To whom correspondence should be addressed. Email: mr@purdue.edu.

This article contains supporting information online at www.pnas.org/lookup/suppl/doi:10.1073/pnas.1815432116/-/DCSupplemental.

Published online January 14, 2019.

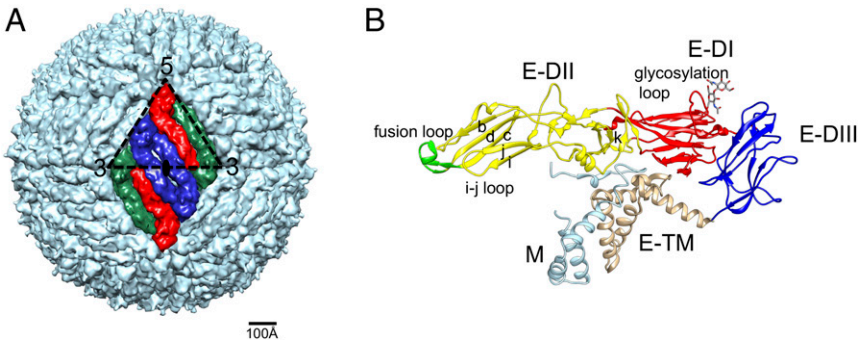

Fig. 1. Structure of mature flaviviruses. (*A*) Surface view of mature ZIKV showing E proteins arranged in a herringbone pattern. The three E protomers within one icosahedral asymmetric unit (outlined by a black triangle) are shown in blue, red, and green. Three E dimers form a raft. (*B*) Ribbon representation of the ZIKV E-M heterodimer. The E protein consists of DI (red), DII (yellow), DIII (blue), and transmembrane domain (TM; tan). The fusion loop of E protein is shown in green. The M protein is shown in light blue.

pr peptide dissociates from the E and M proteins, resulting in the generation of infectious, mature virions (16, 20).

Highly neutralizing, anti-ZIKV antibodies are of significant interest due to their prophylactic and therapeutic potential. Panels of ZIKV neutralizing human monoclonal antibodies (mAbs) have been isolated and studied (21–26). Several neutralizing antibodies previously isolated against DENV showed cross-reactivity against ZIKV, and some had therapeutic activity in mice (27–32). Epitope mapping and structure determinations showed that the majority of type-specific neutralizing epitopes on ZIKV are located on DII and DIII of the E protein (33, 34). Here we analyze the structure–function relationship of the neutralizing human mAb ZIKV-195, which was isolated from a B cell of a subject with a history of prior natural ZIKV infection (22). This mAb exhibited potent neutralizing activity in vitro and showed significant protection against ZIKV infection in a mouse model of infection and disease. Furthermore, we determined the cryo-electron microscopy (cryo-EM) structure of mature ZIKV virus in complex with Fab fragments of ZIKV-195. The footprint of ZIKV-195 included the Asn154 glycosylation loop in DI and the distal regions of DII across two adjacent E protomers within a dimer. Thus, ZIKV neutralization by mAb ZIKV-195 is likely achieved by protecting the fusion loop from exposure and preventing the transition of the E proteins to the fusogenic conformation by cross-linking the E molecules within each raft.

Results and Discussion

Neutralization and Protection Activity of the ZIKV-195 Antibody. The ZIKV-195 mAb broadly inhibits ZIKV strains of African (Dakar 41525 and MR 766), Asian (H/PF/2013 and Malaysia P6740), and American (Paraiba 2015) origin, with 50% half maximal inhibitory (IC_{50}) values in a range of 77–600 ng/mL (Fig. 2*A*). However, ZIKV-195 did not show neutralizing activity against representative strains of the DENV 1–4 serotypes when tested at a concentration of 20 μg/mL. ZIKV-195 showed therapeutic activity in a stringent postexposure protection model in mice against lethal infection. A single 100-μg (5-mg/kg) dose administered at day 5 after ZIKV inoculation significantly reduced rates of lethal infection (Fig. 2*B*). This level of therapeutic protection is comparable to or better than that observed previously with mAbs binding to the cross-reactive E dimer epitope (EDE) or a ZIKV-specific epitope in domain II at the interdimer interface (22, 31).

Cryo-EM Structure of ZIKV Complexed with ZIKV-195 Fab Fragments. To understand the structural basis for its potent activity, purified mature ZIKV strain H/PF/2013 was incubated with excess ZIKV-195 Fab fragments (2 Fab: 1 E molar ratio) at room temperature to form complexes. The virion–Fab complexes were frozen on grids and imaged using a Titan Krios microscope with a Gatan K2 direct electron detector. The particles became spiky in appearance, in contrast to the smooth surface of the native mature unliganded ZIKV, confirming the attachment of the ZIKV-195 Fab fragments to the virions. Similar to most flavivirus preparations for EM studies, some heterogeneity of the particles was observed. After nonreference 2D classification, the classes consisting of broken particles, those lacking icosahedral symmetry, or those lacking an intact lipid layer were discarded. About 21% (a total of 10,687) of the particles were used for 3D reconstruction (*SI Appendix*, Fig. S1*A*). The final cryo-EM map of the ZIKV–Fab complex was determined to a resolution of 4.0 Å, according to the 0.143 Fourier shell correlation criterion (*SI Appendix*, Fig. S1*B*).

The overall cryo-EM map showed good connectivity of density (Fig. 3*A* and *SI Appendix*, Fig. S1*C*). However, the constant domains of the Fab fragments were not well resolved in the density map, suggesting some flexibility of the distal regions of the Fab molecules upon binding to the virus. There were three Fab fragments bound to the E proteins within each icosahedral asymmetric unit, which extended radially from the viral surface. This finding is equivalent to 180 copies of Fab fragments per virion and complete saturation of all available binding sites. However, different contour levels were required to visualize the bound Fab molecules (*SI Appendix*, Fig. S2), suggesting different occupancy of the Fab molecules, which was presumably associated with the chemical differences at the three independent binding sites.

The structure of the E protein (35) was fitted independently into each of the three E protein locations within the icosahedral asymmetric unit of the ZIKV–Fab complex cryo-EM density map. The resultant structure was refined against the experimental density map in real space (*SI Appendix*, Table S1). The superimposition between the E protomers of the complex structure and of the high-resolution native ZIKV structure showed an rmsd of ∼0.9 Å between equivalent Cα atoms. This finding showed that binding of Fab ZIKV-195 to the virus did not induce any significant structural change other than about 10 residues of the i–j loop in the E protein (*SI Appendix*, Fig. S3).

The density map of the complex had lower density in the Fab region than in the E proteins (*SI Appendix*, Table S2). Thus, the bound Fabs did not attain full occupancy. The average density heights of the E proteins and the variable domains of ZIKV-195 Fab were determined using *sumf* in the program EMfit, where *sumf* is the average density height of the fitted atoms (36). The occupancy of each Fab binding site was then estimated as the ratio of the *sumf* value of the variable domain of the bound Fab molecule to the average *sumf* value of the three E monomers in an icosahedral asymmetric unit (*SI Appendix*, Table S2). The occupancy of the Fab fragments closest to the icosahedral fivefold axes was ∼62%, whereas that of the Fab fragments bound closest to the icosahedral twofold axes or threefold axes was ∼37% or ∼23%, respectively. Because there is no obvious steric hindrance between the bound Fab molecules, the difference of occupancy at the three independent binding sites is most likely accounted for by the structural difference of the environment of these binding sites within the same icosahedral asymmetric unit.

Footprint of the ZIKV-195 Antibody. The near-atomic resolution of the density map enabled the building of the Fab structure, especially the complementarity determining regions (CDRs) of the Fab variable domains, which principally contribute to epitope recognition. One Fab molecule of the ZIKV-195 mAb was found to

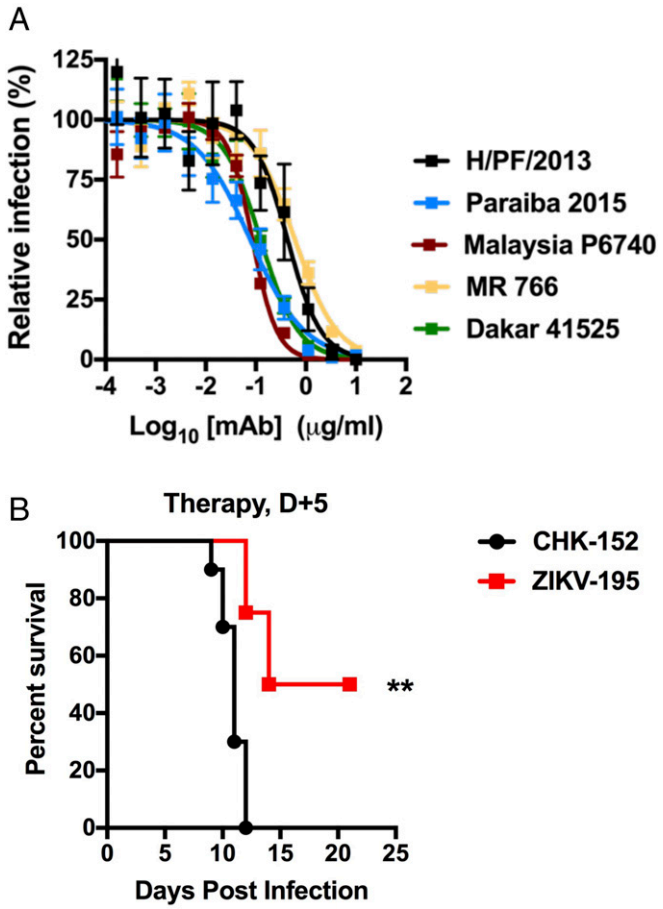

Fig. 2. Functional activity of ZIKV-195. (*A*) Breadth of neutralization activity of ZIKV-195. Indicated ZIKV strains were incubated with increasing concentrations of ZIKV-195 for 1 h at 37 °C before inoculation of Vero cell monolayers. Subsequently, a focus reduction neutralization test was performed. The results are representative of two independent experiments, each performed in triplicate. Error bars indicate SEM. (*B*) Protective, therapeutic activity of ZIKV-195 in adult male mice. Wild-type male 4- to 5-wk-old mice were treated with 1 mg of anti-Ifnar1 mAb followed by s.c. inoculation with 10^5 FFU of ZIKV-Dakar 41525. Mice were treated with a single 100-μg dose of isotype control mAb (hCHK-152) or ZIKV-195 on D + 5 (n = 10 per group from two independent experiments). Significance was analyzed by the log-rank test (**$P < 0.01$).

interact with the two E protomers that form a dimer within a raft (Fig. 3*B*). The total buried area of the interface between the E proteins and the ZIKV-195 Fab is ∼1,400 Å^2. The footprint of the ZIKV-195 Fab on one ZIKV E dimer consists of the b–d strands, the i–j loop, and the fusion loop in DII within one E protomer (E), as well as the Asn154 glycosylation loop in DI, the k strand, and the hinge region of DII in the adjacent E protomer (E′) (Fig. 3*C*). Most of the CDR loops of Fab ZIKV-195 interact with ZIKV E proteins. The contact surface between the heavy (H) chain and the E proteins is about 790 Å^2, whereas the interface between the light (L) chain and the E proteins is about 575 Å^2. Hydrogen bonds and salt bridges are formed between the CDR loops of the H and L chains and the E protomers: (*i*) the L-CDR3 loop of Fab and the Asn154 glycosylation loop of E′-DI; (*ii*) the L-CDR2 and H-CDR3 loops of Fab and the b strand of E-DII; (*iii*) the H-CDR3 loop of Fab and the fusion loop of E-DII; and (*iv*) the H-CDR3, L-CDR1, and L-CDR2 loops of Fab and the i–j loop of E-DII (*SI Appendix*, Table S3).

To corroborate these structural studies and define key amino acid residues important for binding, we mapped the epitope of ZIKV-195 using alanine-scanning shotgun mutagenesis of the prM–E genes coupled with mammalian cell expression and flow cytometry (37). Residues D67, M68, R73, and K251 of the E protein were critical for ZIKV-195 recognition as mutation to alanine resulted in substantial loss-of-binding of ZIKV-195 without disrupting the binding of other conformation-dependent MAbs (Fig. 4*A* and *SI Appendix*, Table S4). These observations are consistent with the cryo-EM results because these residues are located within the ZIKV-195 Fab footprint (Figs. 4*B* and 5).

Although the overall structure of the E proteins of ZIKV in complex with Fab ZIKV-195 is nearly identical to that of the E proteins in the native, uncomplexed ZIKV particle, a structural rearrangement occurs for the i–j loop, which is located in the Fab footprint (*SI Appendix*, Fig. S3). The rmsd between the Cα atoms of the i–j loop in the complex structure and in the native structure is ∼3.6 Å. The quality of the loop density is greatest for the Fab binding sites near the icosahedral fivefold axes and worst for the sites near the icosahedral threefold axes. Furthermore, the quality of the density correlated with the occupancy of the Fab molecules. The i–j loop has large structural differences between some flaviviruses (8, 35). This finding suggests that the i–j loop has greater mobility than other parts of the E protein structure, consistent with its displacement on ZIKV-195 binding. The flexibility of the i–j loop may be used by the ZIKV-195 Fab molecule to create a favorable binding site.

Strand b, the Asn154 glycosylation loop, and the i–j loop of the E protein constitute a large part of the Fab ZIKV-195 epitope. The amino acids in these regions have considerable diversity among flaviviruses but are mostly conserved within different ZIKV strains, providing a basis for the specificity of ZIKV-195 and lack of neutralization of different DENV serotypes (Fig. 2 and *SI Appendix*, Figs. S4 and S5). Because dengue viruses usually have an N-linked glycosylation site at position 67 of the E protein, this glycan would interfere with binding of ZIKV-195.

The exposed solvent accessible regions of the three non-equivalent Fab binding sites in the icosahedral asymmetric unit have areas of ∼1,608, ∼1,499, or ∼1,414 Å^2, for the footprints close to the icosahedral fivefold, twofold, or threefold axes, respectively. The footprints of these three binding sites are composed of similar amino acids but are presented slightly differently, explaining the different occupancies of these sites (Fig. 5).

Structural Insight into the Neutralization Mechanism of ZIKV-195 mAb. Compared with other ZIKV-neutralizing antibodies with known high-resolution structures of the Fab–ZIKV or Fab–ZIKV E complexes (21, 30, 32), the footprint of ZIKV-195 is fairly unique (*SI Appendix*, Fig. S6). The footprint of Fab ZIKV-195 includes multiple secondary structural elements on DI and DII within an E dimer, with E-DII providing ∼89% of the interaction surface. Fab ZIKV-195 binds to both E protomers forming dimers within one icosahedral asymmetric unit, thereby stabilizing the E dimers on the mature ZIKV particle and possibly preventing formation of fusogenic trimers. Furthermore, interaction between Fab ZIKV-195 and the fusion loop of E likely would protect against the structural transitions required for membrane fusion. The conformational transition of the E proteins from dimers to fusogenic trimers is an essential step during virus entry into host cells (38). Thus, binding of ZIKV-195 to the mature ZIKV particle might result in inhibition of membrane fusion.

The Asn154 glycosylation loop of the ZIKV E protein contains an N-linked glycosylation site at residue Asn154, which is conserved among ZIKV, DENV, WNV, and JEV. The Asn154 glycan was reported to be associated with ZIKV virulence and pathogenesis (39, 40). Glycosylation of the E protein at various sites was found to contribute to cell attachment of DENV (41) and pathogenesis of WNV (42). Thus, binding of Fab ZIKV-195 to the Asn154 glycosylation loop of the ZIKV E protein may also hamper infectivity and pathogenicity of the virus.

Antibody-dependent enhancement (ADE) is a potential problem for vaccines or antibody-based therapies that combat infection by flaviviruses (43). In this case, antibodies can enhance viral infection by increasing virion uptake through cellular Fcγ-receptors. Therefore, some E protein antibodies that cross-neutralize ZIKV

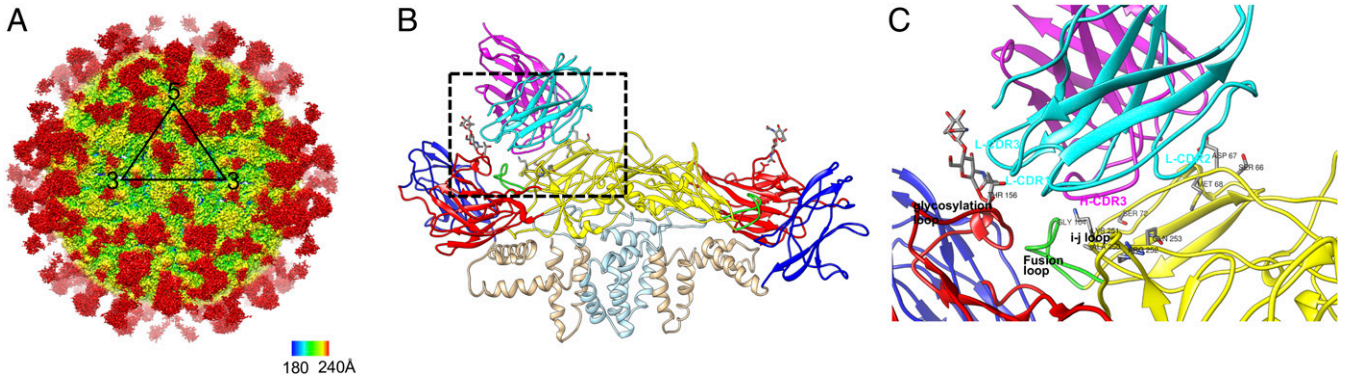

Fig. 3. Structure of ZIKV in complex with Fab ZIKV-195. (*A*) Cryo-EM map of the ZIKV-Fab complex at a contour level of 1.5σ. The map is radially colored. The icosahedral asymmetric unit is outlined by a black triangle. (*B*) Fab variable domain (heavy chain in magenta and light chain in cyan) bound to one E dimer (DI in red, DII in yellow, DIII in blue, and transmembrane domain in tan). Only one Fab of the two Fabs bound to an E dimer is shown for clarity. (*C*) The binding interface, outlined by a rectangle in *B*, is enlarged.

and DENV could increase the risk for ADE (44), if the concentration of antibody were to fall below the stoichiometric threshold required for neutralization (45). ZIKV-195 mAb, because of its specificity, is less likely to enhance infection of heterologous flaviviruses. Thus, the potent neutralizing ZIKV-195 mAb could have therapeutic potential against ZIKV infection with probably low risk of ADE for DENV.

Methods

Viruses. ZIKV strain H/PF/2013 (French Polynesia, 2013) was obtained from X. de Lamballerie (Aix Marseille Université, Marseille, France). ZIKV Brazil Paraiba 2015 was provided by S. Whitehead (National Institutes of Health, Bethesda, MD). ZIKV MR 766 (Uganda, 1947), Malaysia P6740 (1966), and Dakar 41525 (Senegal, 1982) were provided by the World Reference Center for Emerging Viruses and Arboviruses (R. Tesh, University of Texas Medical Branch, Galveston, TX). Both virus stocks of ZIKV and DENV were propagated in Vero cell monolayer cultures. For in vivo studies, ZIKV Dakar 41525 was adapted in mice (46). Virus stocks were titrated by a focus-forming assay on Vero cell monolayer cultures, as described previously (47).

Zika Virus Neutralization Assay. Serial dilutions of mAbs were incubated with ~10^2 FFU of different ZIKV strains for 1 h at 37 °C. The mAb–virus complexes were added to Vero cell monolayers in 96-well plates for 90 min at 37 °C. Subsequently, cells were overlaid with 1% (wt/vol) methylcellulose in MEM supplemented with 4% heat-inactivated FBS. Plates were fixed 40 h later with 1% PFA in PBS for 1 h at room temperature. The plates were incubated sequentially with 500 ng/mL mouse anti-ZIKV (ZV-13) (33) and horseradish-peroxidase–conjugated goat anti-mouse IgG in PBS supplemented with 0.1% (wt/vol) saponin (Sigma) and 0.1% BSA. ZIKV-infected cell foci were visualized using TrueBlue peroxidase substrate (KPL) and quantitated on an ImmunoSpot 5.0.37 macroanalyzer (Cellular Technologies).

Mouse Experiments. This study was carried out in accordance with the recommendations in the *Guide for the Care and Use of Laboratory Animals* of the National Institutes of Health (48). The protocols were approved by the Institutional Animal Care and Use Committee at the Washington University School of Medicine (assurance number A3381-01). Inoculations were performed under anesthesia induced and maintained with ketamine hydrochloride and xylazine, and all efforts were made to minimize animal suffering. The experiments were not randomized, and the investigators were not blinded to allocation during experiments and outcome assessment.

C57BL/6 male mice (4–5 wk old; Jackson Laboratories) were inoculated with 10^5 FFU of ZIKV Dakar 41525 by a s.c. route in the footpad. One day before infection, mice were treated with 1 mg of anti-Ifnar1 mAb (MAR1-5A3; Leinco Technologies) by i.p. injection. ZIKV-specific human mAb (ZIKV-195) or an isotype control (humanized CHK-152) (49) was administered as a single dose at day +5 (100 μg) after infection through an i.p. route.

Cryo-EM Sample Preparation, Data Collection, and 3D Reconstruction. The virus and Fab were prepared following the procedures described previously (7, 22). The ZIKV-195 Fab was mixed with 1 mg/mL of purified mature ZIKV particles at a molar ratio of two Fab fragments per E molecule. The complex was incubated at room temperature for 30 min and transferred on ice before freezing. A 3-μL aliquot of sample was flash frozen on the lacey carbon grid in liquid ethane using a Gatan CP3 plunger. Cryo-EM datasets were collected in multiple sessions using an FEI Titan Krios electron microscope equipped with a Gatan K2 Summit detector. A total of 1,691 micrographs were recorded using the automated software Leginon (50) at 18,000× magnification in the direct counting mode, resulting in a pixel size of 1.62 Å with

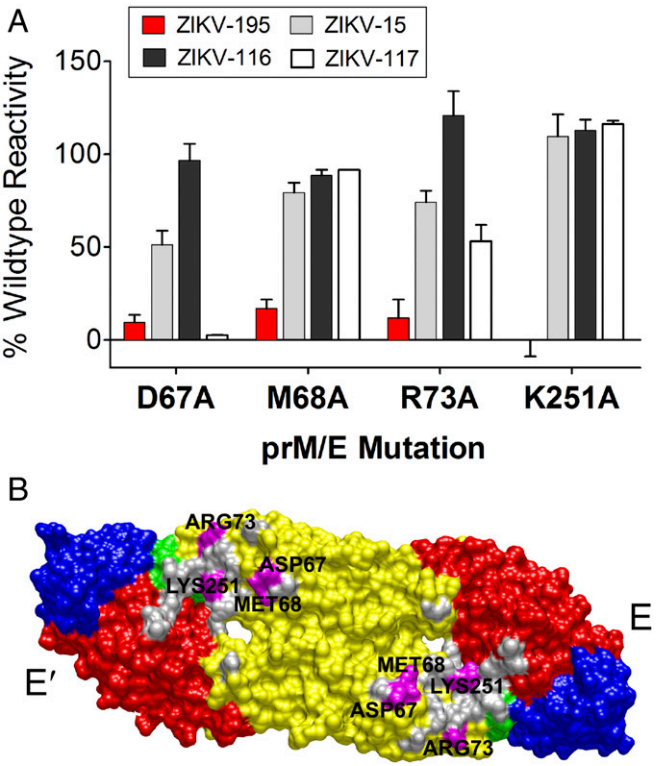

Fig. 4. Alanine scanning epitope mapping of mAb ZIKV-195. (*A*) The mAb reactivity for each alanine mutant of ZIKV prM–E was tested and normalized to reactivity for the wild-type prM–E. Mutants with reactivity less than 30% were identified as critical for mAb binding. The unrelated ZIKV-15, ZIKV-116, and ZIKV-117 mAbs were used as internal controls. Bars were calculated from at least two replicates of independent experiments. (*B*) Comparison of the cryo-EM and alanine mutagenesis mapping for the ZIKV-195 epitopes. Surface top view of the ZIKV E dimer is shown with DI, DII, DIII, and fusion loop colored in red, yellow, blue, and green, respectively. Epitopes identified in the ZIKV-Fab cryo-EM structure are shown in gray, among which critical residues from alanine mutagenesis epitope mapping are shown in magenta.

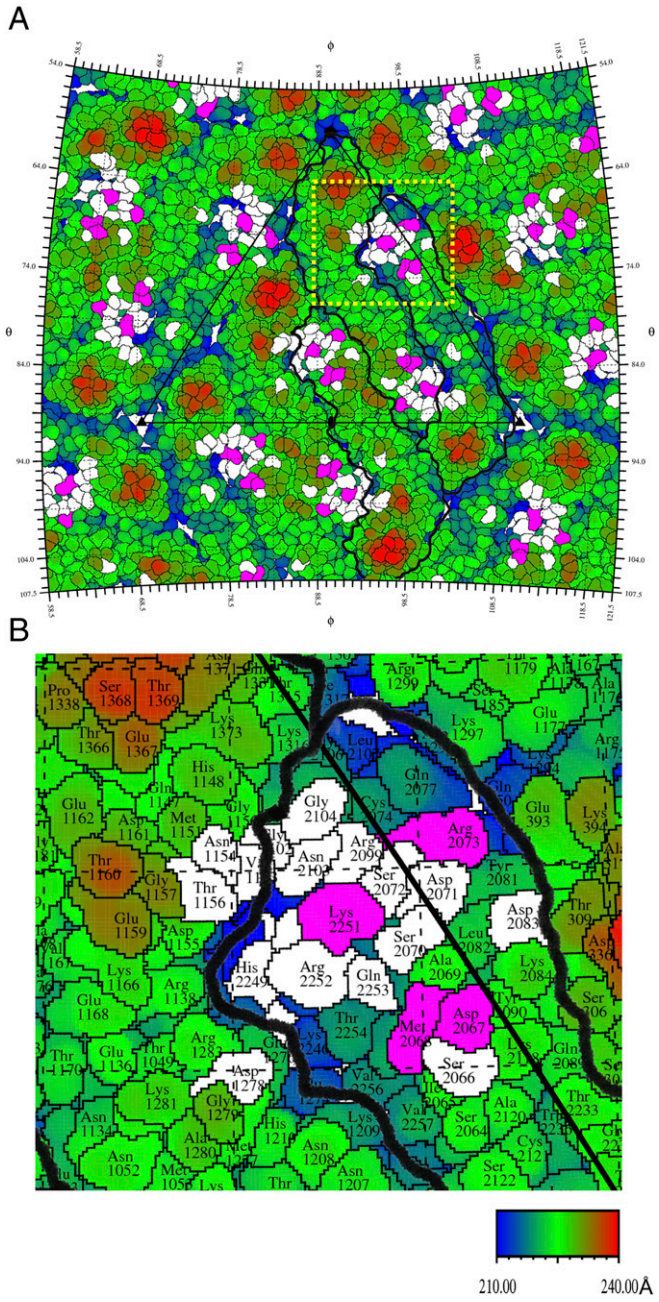

Fig. 5. Roadmap shows footprint of Fab ZIKV-195 on the ZIKV virion. (*A*) The projected surfaces of ZIKV E proteins are colored according to the radial distance of the surface from the virus center. The black triangle denotes the boundary of an icosahedral asymmetric unit. The residues in the Fab footprint (defined by any atoms in the virus less than 4 Å from any atom in the bound Fab) are shown in white, among which the critical residues from alanine mutagenesis epitope mapping are shown in magenta. Three E protomers within one icosahedral asymmetric unit are outlined in black lines. (*B*) The footprint region near the icosahedral fivefold axis, outlined by a yellow rectangle in *A*, is enlarged. Residue numbers of the E protomers closest to the icosahedral twofold, fivefold, or threefold axes are incremented by 0; 1,000; or 2,000, respectively.

total electron dosage of ~30 $e^{-}/Å^2$. The frames of each image were aligned using MotionCorr 2 (51). The contrast transfer function (CTF) of the micrographs was estimated using CTFFIND4 (52). A total of 51,836 particles were boxed using the template-based automatic picking tool in Appion (53). Nonreference 2D classification was performed using RELION (54) and 10,687 "good" particles were selected for 3D reconstruction. The program jspr (55, 56) was used for initial model generation, iterative refinement of center and orientation, and refinement of defocus and astigmatism. According to the gold standard, two independent reconstructions were obtained assuming icosahedral symmetry from two half datasets that were split from the start of the procedure. The final reconstruction was generated by combining the two half datasets after the refinement had converged. The overall resolution was 4.1 Å (unmasked) and 4.0 Å (masked by removing the internal nucleic acid region and the external background region), using the Fourier shell correlation criterion of 0.143 (57). The resulting cryo-EM map was sharpened further using the postprocess procedure in RELION.

Structure Fitting, Refinement, and Analysis. An initial model of the variable domain of ZIKV-195 mAb was predicted based on the known protein sequence using the program PIGS (58). The bound Fab that was closest to the icosahedral fivefold vertex had the best quality of density and thus was used for manual model rebuilding of the variable domain using the graphics computer program COOT (59) and the real space refinement feature in the computer program PHENIX (60). The coordinates of the E proteins obtained from a 3.1-Å-resolution cryo-EM map of ZIKV [Protein Data Bank (PDB) ID: 6CO8] (35) were fitted into the map and refined in real space using PHENIX. The structures were analyzed with the Chimera (61) and PyMOL (https://pymol.org/2/) programs. The molecular contacts were analyzed using the programs NCONT in CCP4 (59) and PISA (62). The superimpositions of structures were performed using the program HOMOLOGY (63). All rmsd values were calculated using the Cα atom coordinates. Roadmaps of the Fab footprints were plotted using the program RIVEM (64).

Determination of Fab Occupancy. Fab occupancy was estimated by comparison of density height using the program EMfit (36). The *sumf* values (the normalized mean density of the fitted atoms) of E and Fab variable domains were calculated using EMfit. The $sumf_E$ value represents full occupancy. Thus, the ratio of $sumf_{Fab}$ to $sumf_E$ represents the occupancy of Fab.

Alanine Scanning Epitope Mapping. Epitope mapping by alanine-scanning mutagenesis was performed as described previously (22, 37). A ZIKV prM–E protein expression construct (strain SPH2015) was subjected to high-throughput alanine scanning mutagenesis to generate a comprehensive mutation library. Each residue within prM–E was mutated to alanine, except for alanines, which were mutated to serines. In total, 672 ZIKV prM–E mutants were generated and expressed transiently in HEK293T cells for 22 h in 384-well plates. Cells expressing the protein mutants were fixed in 4% (vol/vol) paraformaldehyde (Electron Microscopy Sciences) and permeabilized with 0.1% (wt/vol) saponin (Sigma-Aldrich) in PBS plus calcium and magnesium (PBS++) buffer. Cells were sequentially incubated with 2.0 μg/mL purified ZIKV-195 mAb and 3.75 μg/mL of Alexa Fluor 488-conjugated secondary antibody (Jackson ImmunoResearch Laboratories), which were diluted in PBS++, 10% normal goat serum (Sigma), and 0.1% saponin. After cells were washed three times with PBS++/0.1% saponin and additionally twice with PBS, mean cellular fluorescence was recorded using a high-throughput flow cytometer (Intellicyt). Antibody reactivity against each prM–E mutant relative to the wild-type protein was calculated by subtracting the signal from mock-transfected controls and normalizing to the signal from wild-type prM–E-transfected controls.

Statistical Analysis. All virological data were analyzed with GraphPad Prism software. Kaplan–Meier survival curves were analyzed by the log rank test. $P < 0.05$ indicated statistically significant differences.

Protein Sequence Alignment and Annotation. Protein sequence alignments were conducted using the program CLUSTALW of the web server Network Protein Sequence analysis (NPS@) (https://npsa-prabi.ibcp.fr). The alignment figures were prepared using the web server ESPript (65). The ZIKV E ectodomain consists of DI (residues 1–52, 131–192, and 287–305), DII (residues 53–130 and 193–286), and DIII (residues 306–404). The fusion loop of E consists of residues 98–109.

ACKNOWLEDGMENTS. We thank Sheryl Kelly for help in preparing the manuscript. We thank Geeta Buda for help with cell culture as well as Yingyuan Sun and Yue Liu for their help with cryo-EM data collection and for further discussion. We thank members of the J.E.C. research laboratory (Vanderbilt University Medical Center) for their technical support, including Robin Bombardi (antibody sequence analysis, Fab synthesis, and cloning), Nurgun Kose (ELISA verification of mAb binding), Rachel Nargi (production of recombinant IgG and Fab molecules), Dina Yousif (IgG purification), and Robert Carnahan and Merissa Mayo (antibody project oversight). Cryo-EM data were collected at the Purdue University Cryo-EM Facility. The computation was supported, in part, through computational resources provided by

Information Technology Research Computing at Purdue University, West Lafayette, Indiana. This work was supported by US National Institutes of Health (NIH) Grants R01 AI076331 (to M.G.R. and R.J.K.), NIH R01 AI127828 (to J.E.C. and M.S.D.), NIH R01 AI073755 (to M.S.D.; subawards to M.G.R., J.E.C., and R.J.K.), NIH R01 AI104972 (to M.S.D.), HHSN272201400024C (to J.E.C.), and HHSN272201400058C (to B.J.D.).

1. Simmonds P, et al.; Ictv Report Consortium (2017) ICTV virus taxonomy profile: Flaviviridae. *J Gen Virol* 98:2–3.
2. Gregory CJ, et al. (2017) Modes of transmission of Zika virus. *J Infect Dis* 216: S875–S883.
3. Samarasekera U, Triunfol M (2016) Concern over Zika virus grips the world. *Lancet* 387:521–524.
4. Available at https://wwwnc.cdc.gov/travel/page/zika-travel-information.
5. Cao-Lormeau VM, et al. (2016) Guillain-Barré syndrome outbreak associated with Zika virus infection in French Polynesia: A case-control study. *Lancet* 387:1531–1539.
6. Mlakar J, et al. (2016) Zika virus associated with microcephaly. *N Engl J Med* 374: 951–958.
7. Sirohi D, et al. (2016) The 3.8 Å resolution cryo-EM structure of Zika virus. *Science* 352: 467–470.
8. Wang X, et al. (2017) Near-atomic structure of Japanese encephalitis virus reveals critical determinants of virulence and stability. *Nat Commun* 8:14.
9. Kostyuchenko VA, et al. (2016) Structure of the thermally stable Zika virus. *Nature* 533:425–428.
10. Zhang X, et al. (2013) Cryo-EM structure of the mature dengue virus at 3.5-Å resolution. *Nat Struct Mol Biol* 20:105–110.
11. Füzik T, et al. (2018) Structure of tick-borne encephalitis virus and its neutralization by a monoclonal antibody. *Nat Commun* 9:436.
12. Zhang X, et al. (2013) Dengue structure differs at the temperatures of its human and mosquito hosts. *Proc Natl Acad Sci USA* 110:6795–6799.
13. Fibriansah G, et al. (2013) Structural changes in dengue virus when exposed to a temperature of 37 °C. *J Virol* 87:7585–7592.
14. Rey FA, Heinz FX, Mandl C, Kunz C, Harrison SC (1995) The envelope glycoprotein from tick-borne encephalitis virus at 2 A resolution. *Nature* 375:291–298.
15. Kuhn RJ, et al. (2002) Structure of dengue virus: Implications for flavivirus organization, maturation, and fusion. *Cell* 108:717–725.
16. Li L, et al. (2008) The flavivirus precursor membrane-envelope protein complex: Structure and maturation. *Science* 319:1830–1834.
17. Sirohi D, Kuhn RJ (2017) Zika virus structure, maturation, and receptors. *J Infect Dis* 216:S935–S944.
18. Zhang Y, et al. (2004) Conformational changes of the flavivirus E glycoprotein. *Structure* 12:1607–1618.
19. Prasad VM, et al. (2017) Structure of the immature Zika virus at 9 Å resolution. *Nat Struct Mol Biol* 24:184–186.
20. Yu IM, et al. (2008) Structure of the immature dengue virus at low pH primes proteolytic maturation. *Science* 319:1834–1837.
21. Wang Q, et al. (2016) Molecular determinants of human neutralizing antibodies isolated from a patient infected with Zika virus. *Sci Transl Med* 8:369ra179.
22. Sapparapu G, et al. (2016) Neutralizing human antibodies prevent Zika virus replication and fetal disease in mice. *Nature* 540:443–447.
23. Stettler K, et al. (2016) Specificity, cross-reactivity, and function of antibodies elicited by Zika virus infection. *Science* 353:823–826.
24. Robbiani DF, et al. (2017) Recurrent potent human neutralizing antibodies to Zika virus in Brazil and Mexico. *Cell* 169:597–609.e11.
25. Magnani DM, et al. (2017) Neutralizing human monoclonal antibodies prevent Zika virus infection in macaques. *Sci Transl Med* 9:eaan8184.
26. Wang J, et al. (2017) A human bi-specific antibody against Zika virus with high therapeutic potential. *Cell* 171:229–241.e15.
27. Swanstrom JA, et al. (2016) Dengue virus envelope dimer epitope monoclonal antibodies isolated from dengue patients are protective against Zika virus. *MBio* 7:e01123-16.
28. Priyamvada L, et al. (2016) Human antibody responses after dengue virus infection are highly cross-reactive to Zika virus. *Proc Natl Acad Sci USA* 113:7852–7857.
29. Dai L, et al. (2016) Structures of the Zika virus envelope protein and its complex with a flavivirus broadly protective antibody. *Cell Host Microbe* 19:696–704.
30. Barba-Spaeth G, et al. (2016) Structural basis of potent Zika-dengue virus antibody cross-neutralization. *Nature* 536:48–53.
31. Fernandez E, et al. (2017) Human antibodies to the dengue virus E-dimer epitope have therapeutic activity against Zika virus infection. *Nat Immunol* 18:1261–1269.
32. Zhang S, et al. (2016) Neutralization mechanism of a highly potent antibody against Zika virus. *Nat Commun* 7:13679.
33. Zhao H, et al. (2016) Structural basis of Zika virus-specific antibody protection. *Cell* 166:1016–1027.
34. Hasan SS, et al. (2017) A human antibody against Zika virus crosslinks the E protein to prevent infection. *Nat Commun* 8:14722.
35. Sevvana M, et al. (2018) Refinement and analysis of the mature Zika virus cryo-EM structure at 3.1 Å resolution. *Structure* 26:1169–1177.e3.
36. Rossmann MG, Bernal R, Pletnev SV (2001) Combining electron microscopic with x-ray crystallographic structures. *J Struct Biol* 136:190–200.
37. Davidson E, Doranz BJ (2014) A high-throughput shotgun mutagenesis approach to mapping B-cell antibody epitopes. *Immunology* 143:13–20.
38. Mukhopadhyay S, Kuhn RJ, Rossmann MG (2005) A structural perspective of the flavivirus life cycle. *Nat Rev Microbiol* 3:13–22.
39. Annamalai AS, et al. (2017) Zika virus encoding non-glycosylated envelope protein is attenuated and defective in neuroinvasion. *J Virol* 91:e01348-17.
40. Fontes-Garfias CR, et al. (2017) Functional analysis of glycosylation of Zika virus envelope protein. *Cell Rep* 21:1180–1190.
41. Pokidysheva E, et al. (2006) Cryo-EM reconstruction of dengue virus in complex with the carbohydrate recognition domain of DC-SIGN. *Cell* 124:485–493.
42. Beasley DWC, et al. (2005) Envelope protein glycosylation status influences mouse neuroinvasion phenotype of genetic lineage 1 West Nile virus strains. *J Virol* 79:8339–8347.
43. Halstead SB (2003) Neutralization and antibody-dependent enhancement of dengue viruses. *Adv Virus Res* 60:421–467.
44. Dejnirattisai W, et al. (2016) Dengue virus sero-cross-reactivity drives antibody-dependent enhancement of infection with zika virus. *Nat Immunol* 17:1102–1108.
45. Pierson TC, et al. (2007) The stoichiometry of antibody-mediated neutralization and enhancement of West Nile virus infection. *Cell Host Microbe* 1:135–145.
46. Gorman MJ, et al. (2018) An immunocompetent mouse model of Zika virus infection. *Cell Host Microbe* 23:672–685.e6.
47. Brien JD, Lazear HM, Diamond MS (2013) Propagation, quantification, detection, and storage of West Nile virus. *Curr Protoc Microbiol* 31:15D.3.1–15D.3.18.
48. National Research Council (2011) *Guide for the Care and Use of Laboratory Animals* (National Academies Press, Washington, DC), 8th Ed.
49. Pal P, et al. (2013) Development of a highly protective combination monoclonal antibody therapy against Chikungunya virus. *PLoS Pathog* 9:e1003312.
50. Suloway C, et al. (2005) Automated molecular microscopy: The new Leginon system. *J Struct Biol* 151:41–60.
51. Zheng SQ, et al. (2017) MotionCor2: Anisotropic correction of beam-induced motion for improved cryo-electron microscopy. *Nat Methods* 14:331–332.
52. Rohou A, Grigorieff N (2015) CTFFIND4: Fast and accurate defocus estimation from electron micrographs. *J Struct Biol* 192:216–221.
53. Lander GC, et al. (2009) Appion: An integrated, database-driven pipeline to facilitate EM image processing. *J Struct Biol* 166:95–102.
54. Scheres SH (2012) RELION: Implementation of a Bayesian approach to cryo-EM structure determination. *J Struct Biol* 180:519–530.
55. Yu G, et al. (2016) An algorithm for estimation and correction of anisotropic magnification distortion of cryo-EM images without need of pre-calibration. *J Struct Biol* 195:207–215.
56. Guo F, Jiang W (2014) Single particle cryo-electron microscopy and 3-D reconstruction of viruses. *Methods Mol Biol* 1117:401–443.
57. Rosenthal PB, Henderson R (2003) Optimal determination of particle orientation, absolute hand, and contrast loss in single-particle electron cryomicroscopy. *J Mol Biol* 333:721–745.
58. Marcatili P, Rosi A, Tramontano A (2008) PIGS: Automatic prediction of antibody structures. *Bioinformatics* 24:1953–1954.
59. Potterton L, et al. (2004) Developments in the CCP4 molecular-graphics project. *Acta Crystallogr D Biol Crystallogr* 60:2288–2294.
60. Adams PD, et al. (2010) PHENIX: A comprehensive Python-based system for macromolecular structure solution. *Acta Crystallogr D Biol Crystallogr* 66:213–221.
61. Pettersen EF, et al. (2004) UCSF Chimera–A visualization system for exploratory research and analysis. *J Comput Chem* 25:1605–1612.
62. Krissinel E, Henrick K (2007) Inference of macromolecular assemblies from crystalline state. *J Mol Biol* 372:774–797.
63. Rossmann MG, Argos P (1976) Exploring structural homology of proteins. *J Mol Biol* 105:75–95.
64. Xiao C, Rossmann MG (2007) Interpretation of electron density with stereographic roadmap projections. *J Struct Biol* 158:182–187.
65. Robert X, Gouet P (2014) Deciphering key features in protein structures with the new ENDscript server. *Nucleic Acids Res* 42:W320–W24.